Supporting information

Sulfonic acid modified hollow polymer nanospheres with tunable wall-thickness for improving biodiesel synthesis efficiency

Wenliang Song, Yu Zhang, Anuraj Varyambath, Ji Su Kim and Il Kim*

BK21 PLUS Centre for Advanced Chemical Technology, Department of Polymer Science and Engineering, Pusan National University, Pusan 609-735, Republic of Korea.

Contents

Results and Discussion

Fig. S1. The hypothetic mechanism for form the HHPB-IC-- S2

Fig. S2. The hypothetic mechanism for form the HHPB-SA--S2

Fig. S3. Energy-dispersive X-ray spectroscopy (EDX) spectra images for the (a) SHPB-SA, (b) SHPN-SA, (c) SHPB-IC, and (d) SHPN-IC-- S3

Fig. S4. High-angle annular dark field scanning transmission electron microscopy (HAADF-STEM) images and EDS line scan images of the SHPB-SA and SHPN-SA------------------------- S4

Fig. S5. High-angle annular dark field scanning transmission electron microscopy (HAADF-STEM) images and EDS line scan images of the SHPB-IC and SHPN-IC----------- --------------S5

Fig. S6. The TEM images of the HHPB-SA and the SHPB-SA, it can be observed from the figure that the 3D cross-linked hollow structures are well maintained after the sulfonation---------------S6

Fig. S7. The N_2 adsorption and desorption isotherms for HHPs at 77.3 K--------------------------- S6

Fig. S8. Swelling ability of the HHPs and SHPs---S7

Fig. S9. SHPB-SA catalyzed reaction mechanism of esterification reaction------------------------S8

Fig. S10. SHPB-SA catalyzed reaction mechanism of transesterification reaction----------------- S9

Fig. S11. The SEM and TEM images of recycled SHNP-SA --------------------------------------- S10

Fig. S12. The FT-IR spectrum of the recycled SHNP-SA-- S10

Fig. S13. The BET surface area measurement of the recycled SHPB-SA--------------------------- S10

Fig. S14. The EDX mapping results of of the recycled SHPB-SA ---------------------------------- S12

Fig. S15. The ^{1}H NMR and ^{13}C NMR spectra of the lauric acid methyl ester---------------------- S13

Fig. S16. The ^{1}H NMR and ^{13}C NMR spectra of the lauric acid ethyl ester------------------------

S14
Fig. S17. The ^{1}H NMR and ^{13}C NMR spectra of the lauric acid butyl ester------------------------S15
Fig. S18. The ^{1}H NMR and ^{13}C NMR spectra of the coconut oil methyl ester---------------------S16
Fig. S19. The ^{1}H NMR and ^{13}C NMR spectra of the palm oil methyl ester------------------------S17
Fig. S20. The ^{1}H NMR and ^{13}C NMR spectra of the soybean oil methyl ester---------------------S18
Fig. S21. The ^{1}H NMR and ^{13}C NMR spectra of the waste oil methyl ester------------------------S19
Table S1. Conventional method for synthesis the hollow polymer spheres with tunable wall-thickness---S20
Table S2. The EDX results of the SHSPs before and after the transesterification reactions-----S21
References ---S21

Results and Discussion

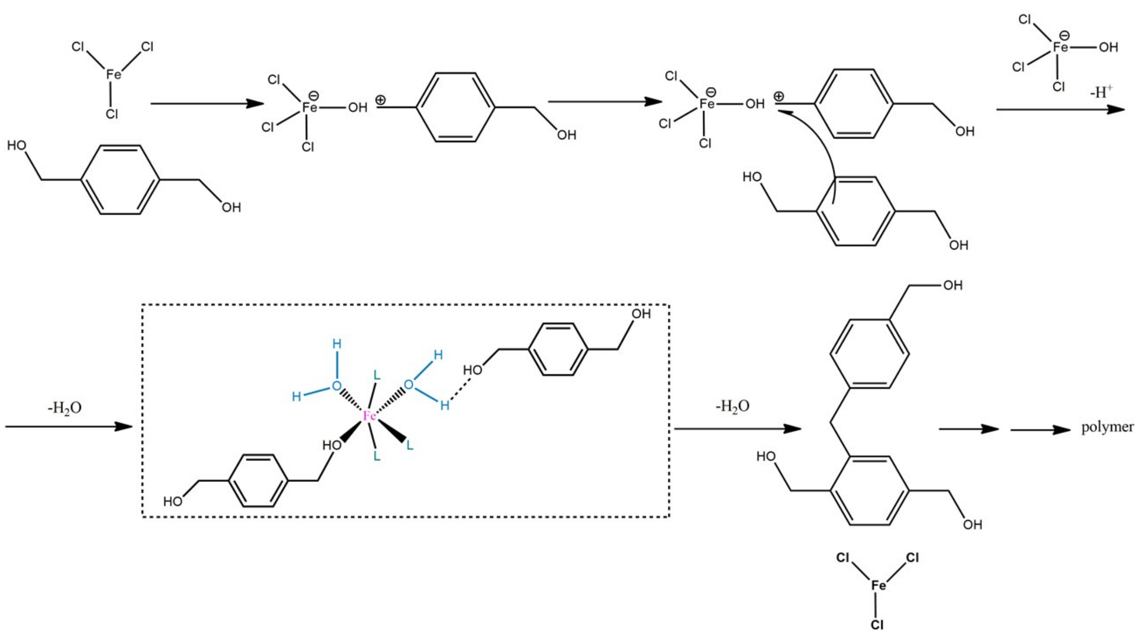

Fig. S1. The hypothetic mechanism for form the HHPB-IC, and the hydrogen bonding forming between the acid and base will balance the strong interactions. L represents either a ligand coordinated to iron or a vacant coordination site of iron.

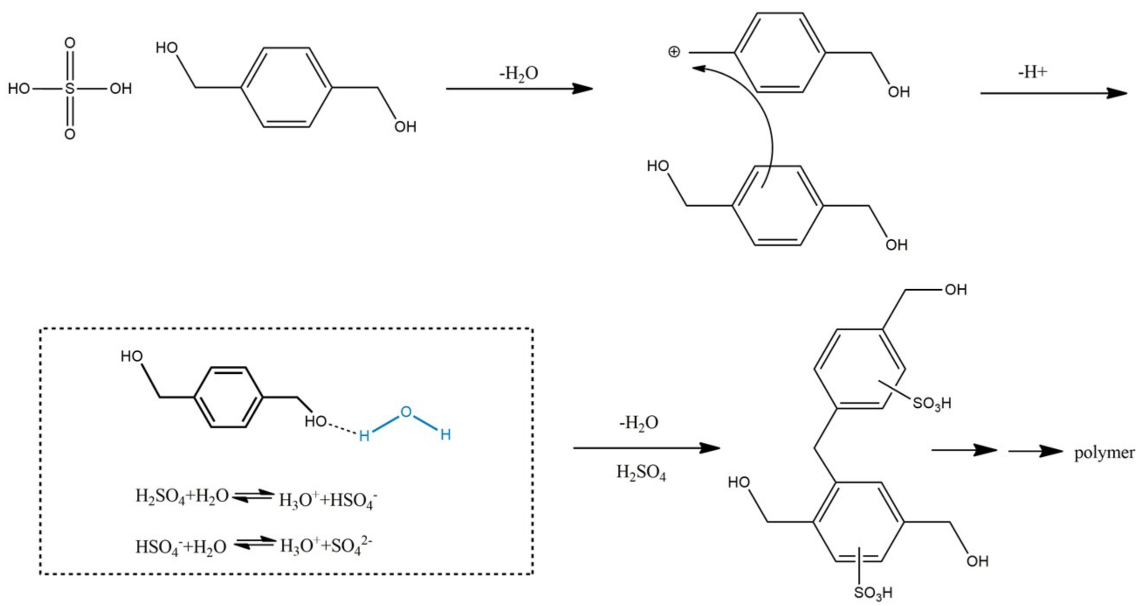

Fig. S2. The hypothetic mechanism for form the HHPB-SA, and the hydrogen bonding forming between the acid and base will balance the strong interactions. The side reaction happens at the same time, which result practical sulfonation during the polymerization process, and the morphology of HHPB-SA are not uniform as the HHPB-IC.

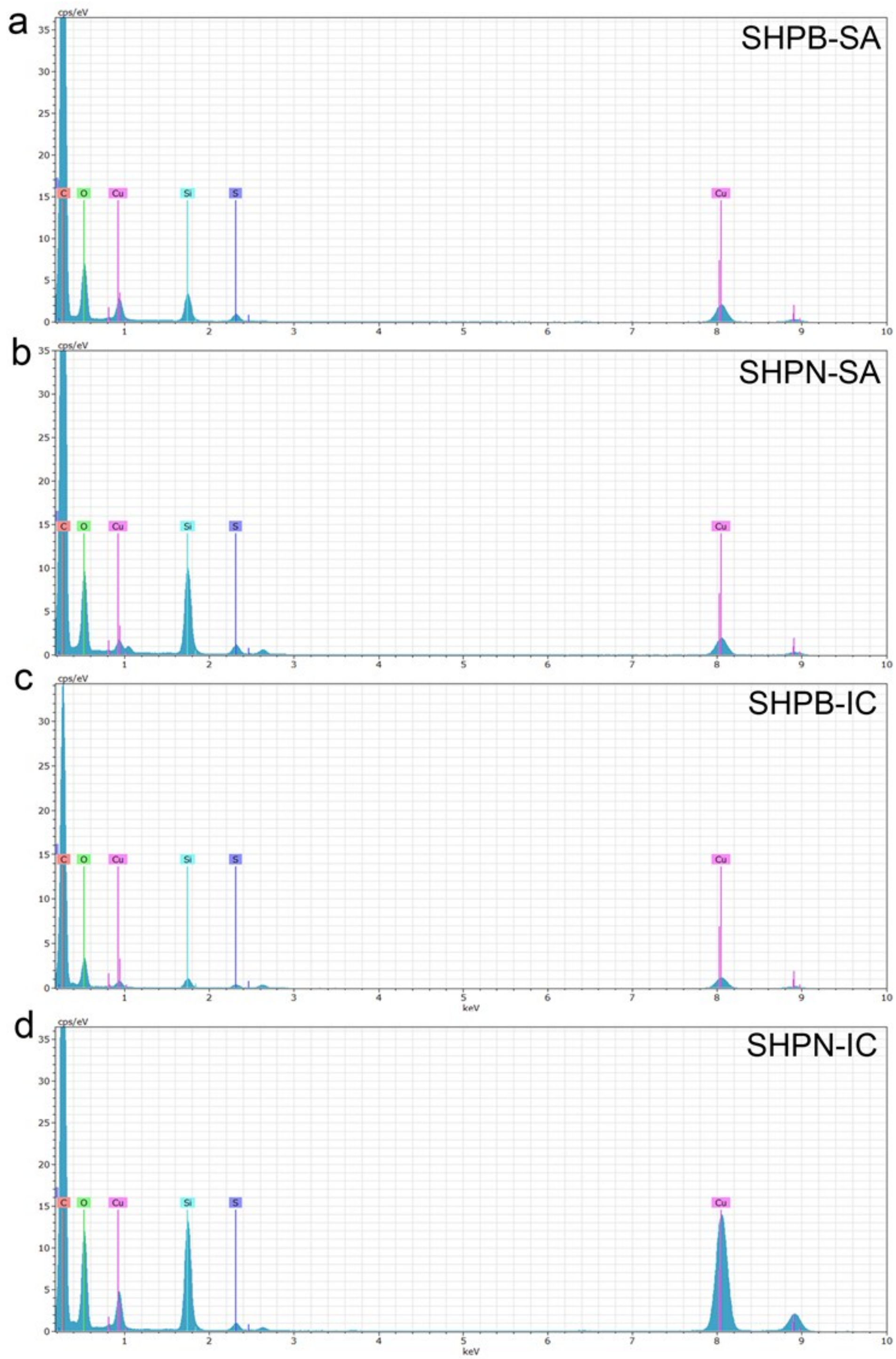

Fig. S3. Energy-dispersive X-ray spectroscopy (EDX) spectra images for the (a) SHPB-SA, (b) SHPN-SA, (c) SHPB-IC, and (d) SHPN-IC. It can be seen that the peaks related to the C, O, S, Si, Cu were shown on the images of the sulfonated samples. Where the Cu peaks are from the mesh of TEM grids and the Si peak is from the background.

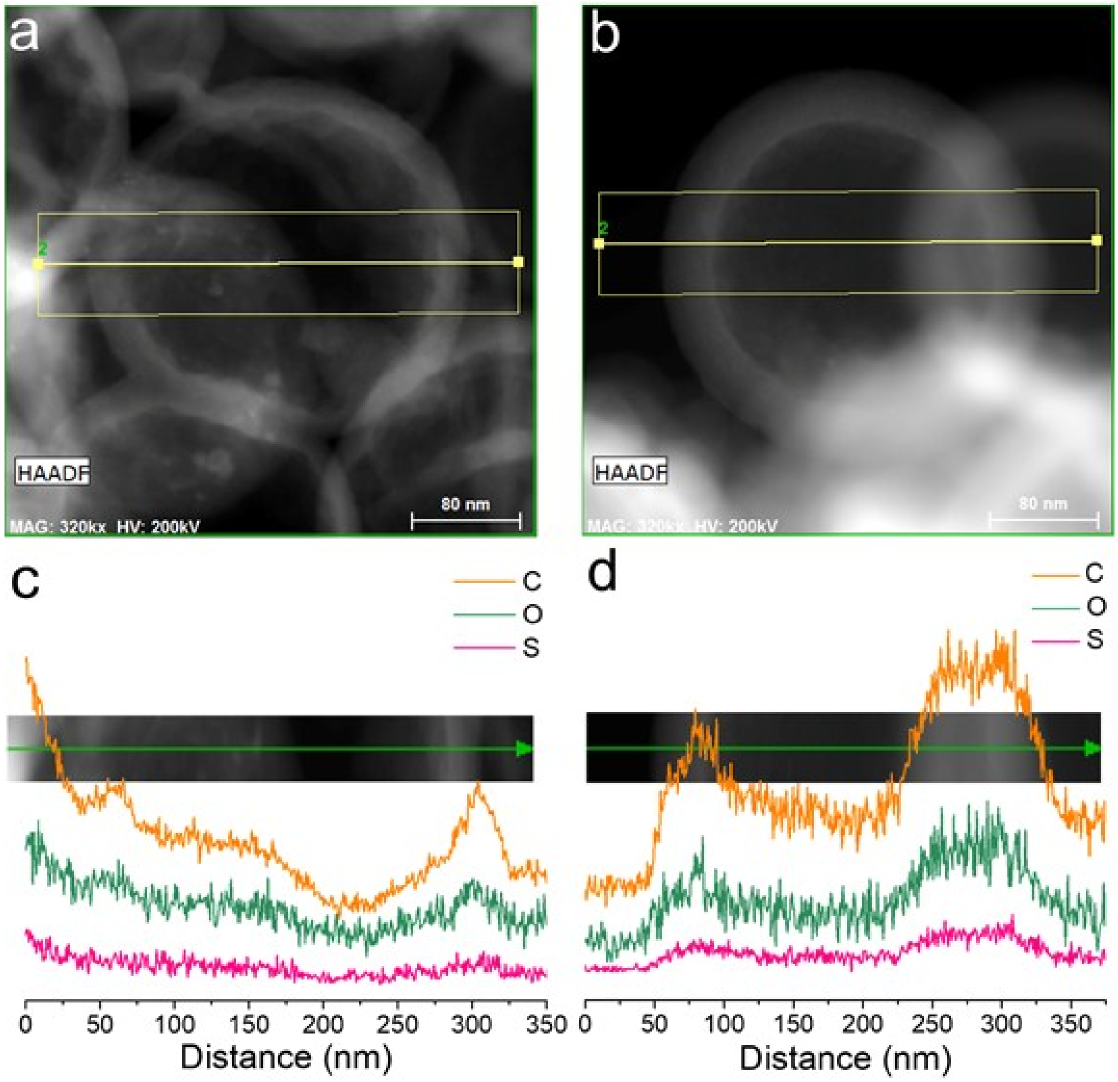

Fig. S4. High-angle annular dark field scanning transmission electron microscopy (HAADF-STEM) images and EDS line scan images of the SHPB-SA and SHPN-SA. The results of (a, c) SHPB-SA and (b, d) SHPN-SA, showing the hollow structures are keep well after the hazardous sulfonation process, and the it also shows the different thickness of hollow spheres.

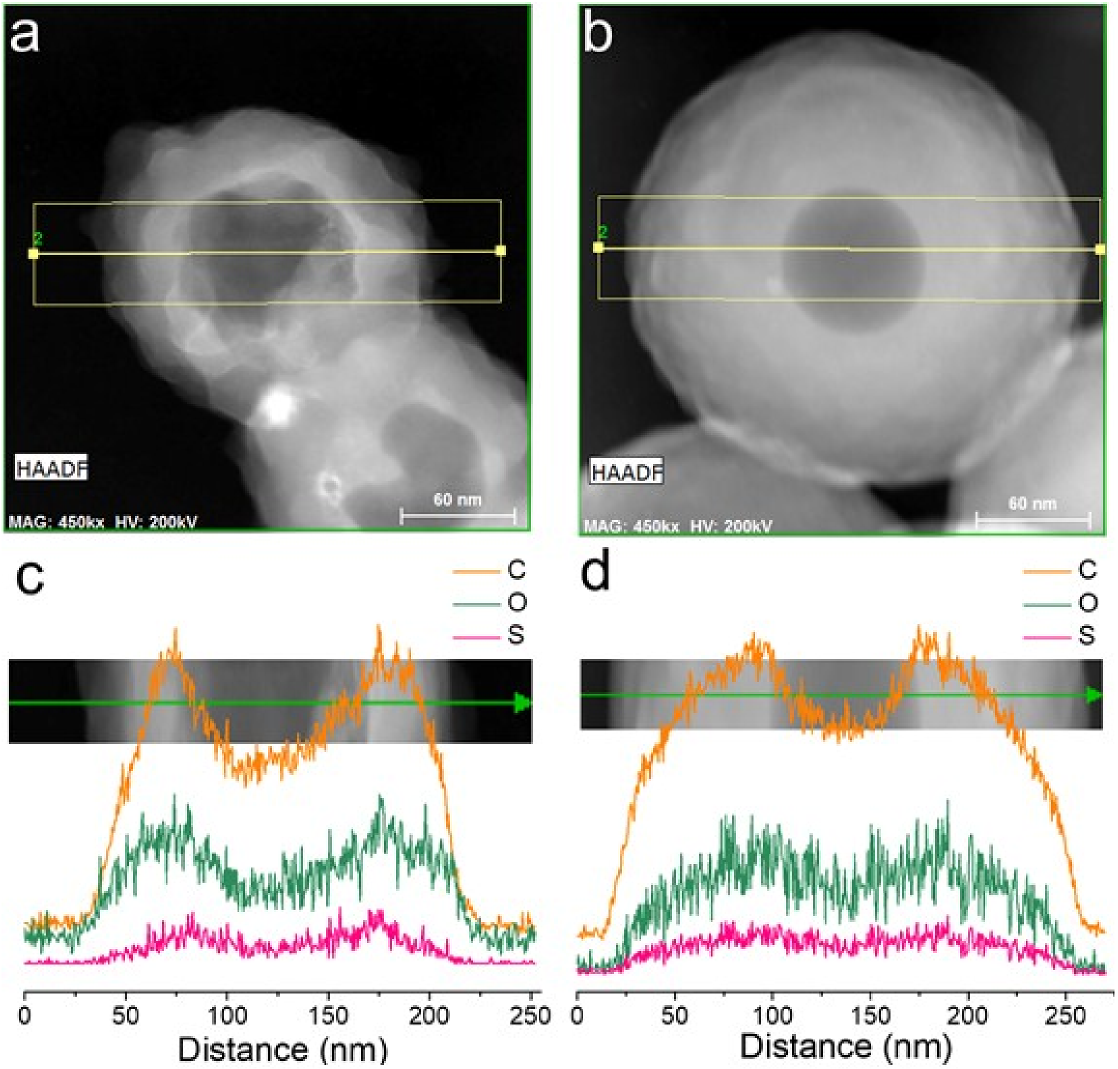

Fig. S5. High-angle annular dark field scanning transmission electron microscopy (HAADF-STEM) images and EDS line scan images of the SHPB-IC and SHPN-IC. The results of (a, c) SHPB-IC and (b, d) SHPN-IC, showing the hollow structures are keep well after the hazardous sulfonation process, and the it also shows the different thickness of hollow spheres.

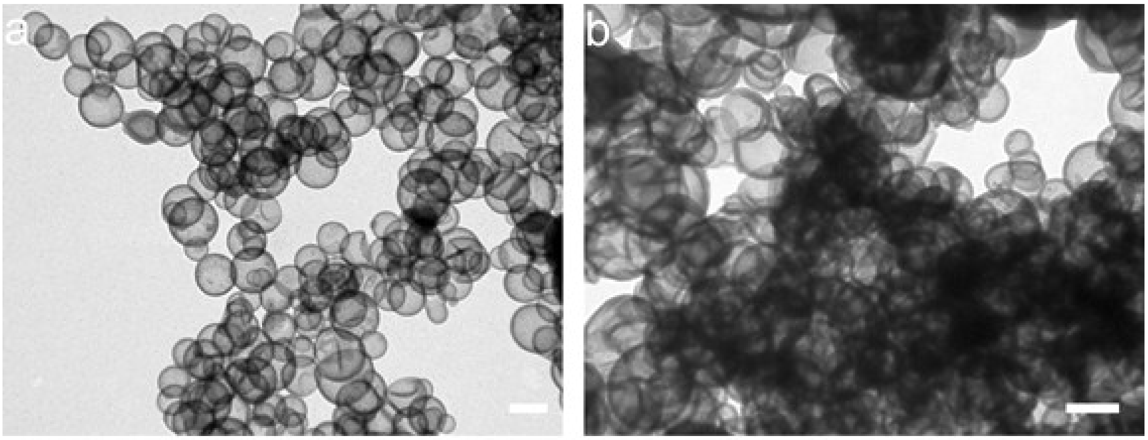

Fig. S6. The TEM images of the HHPB-SA and the SHPB-SA, it can be observed from the figure that the 3D cross-linked hollow structures are well maintained after the sulfonation.

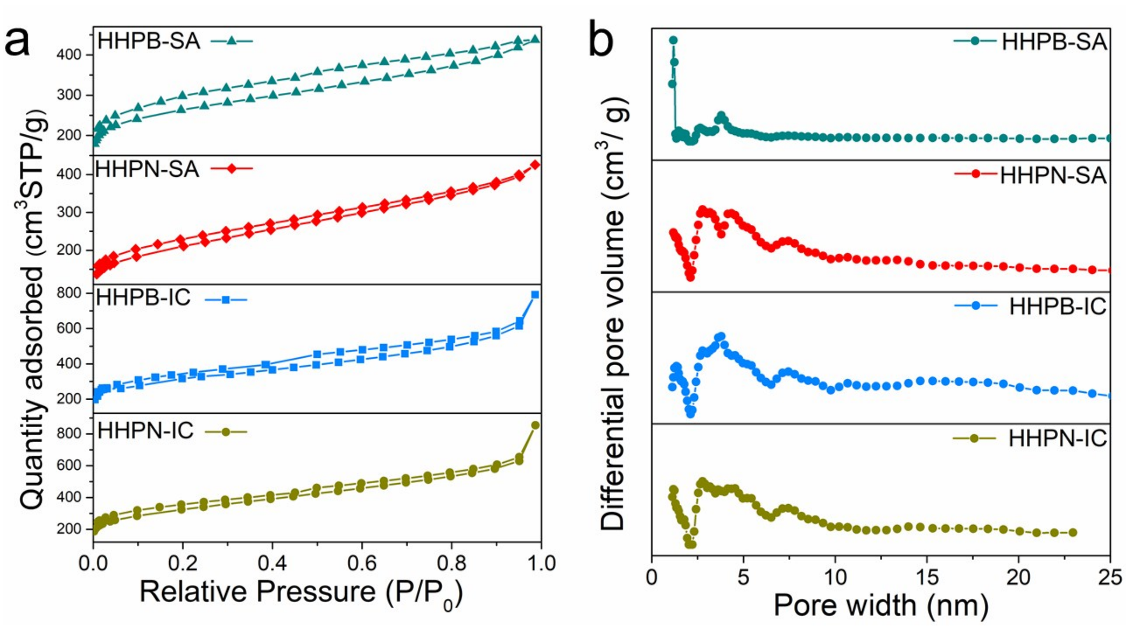

Fig. S7. The N_2 adsorption and desorption isotherms for HHPs at 77.3 K (a), pore size distribution curves for HHPs calculated by NL-DFT method (b).

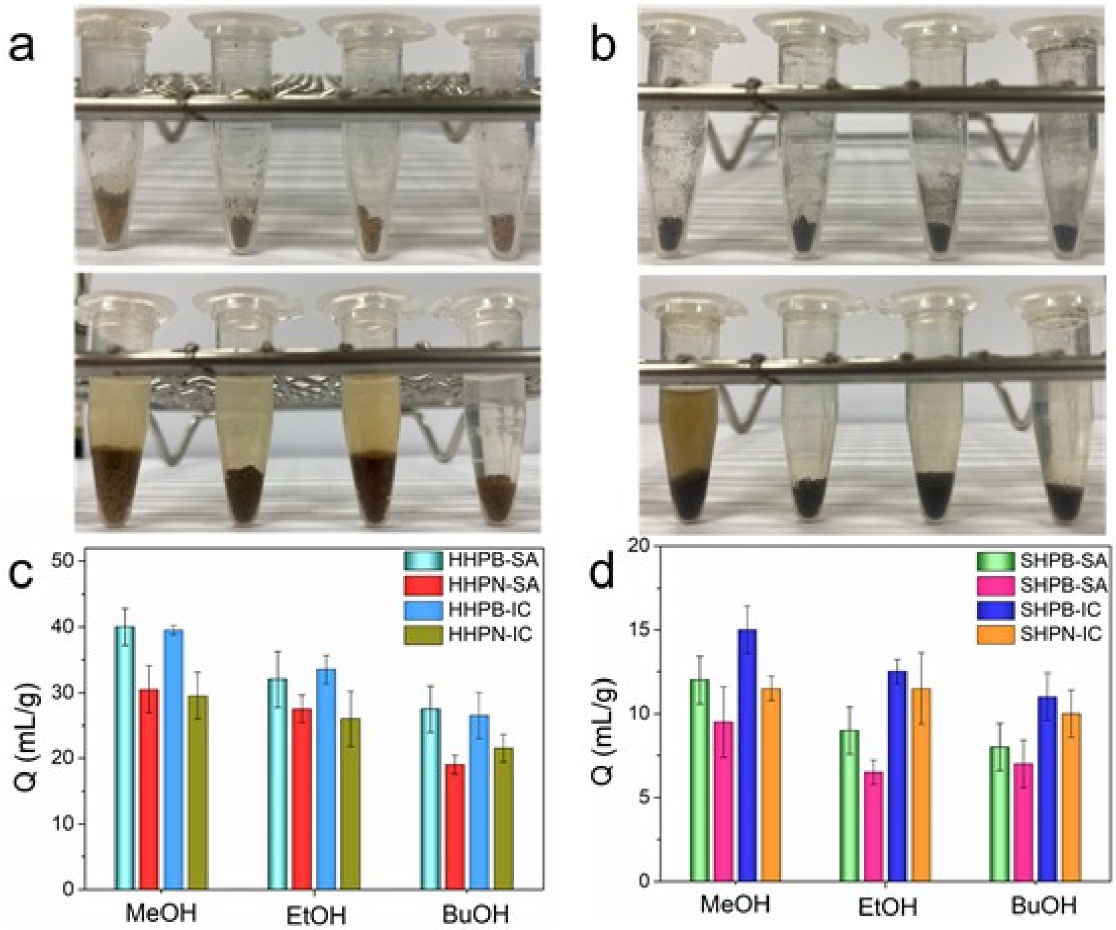

Fig. S8. Swelling ability of the HHPs and SHPs. a, b the optical photograph showing the swelling ability test of HHPs (a) and SHPs (b) against MeOH. c, d the swelling ability of the HHPs (c) and SHPs (d) against MeOH, EtOH, and BuOH.

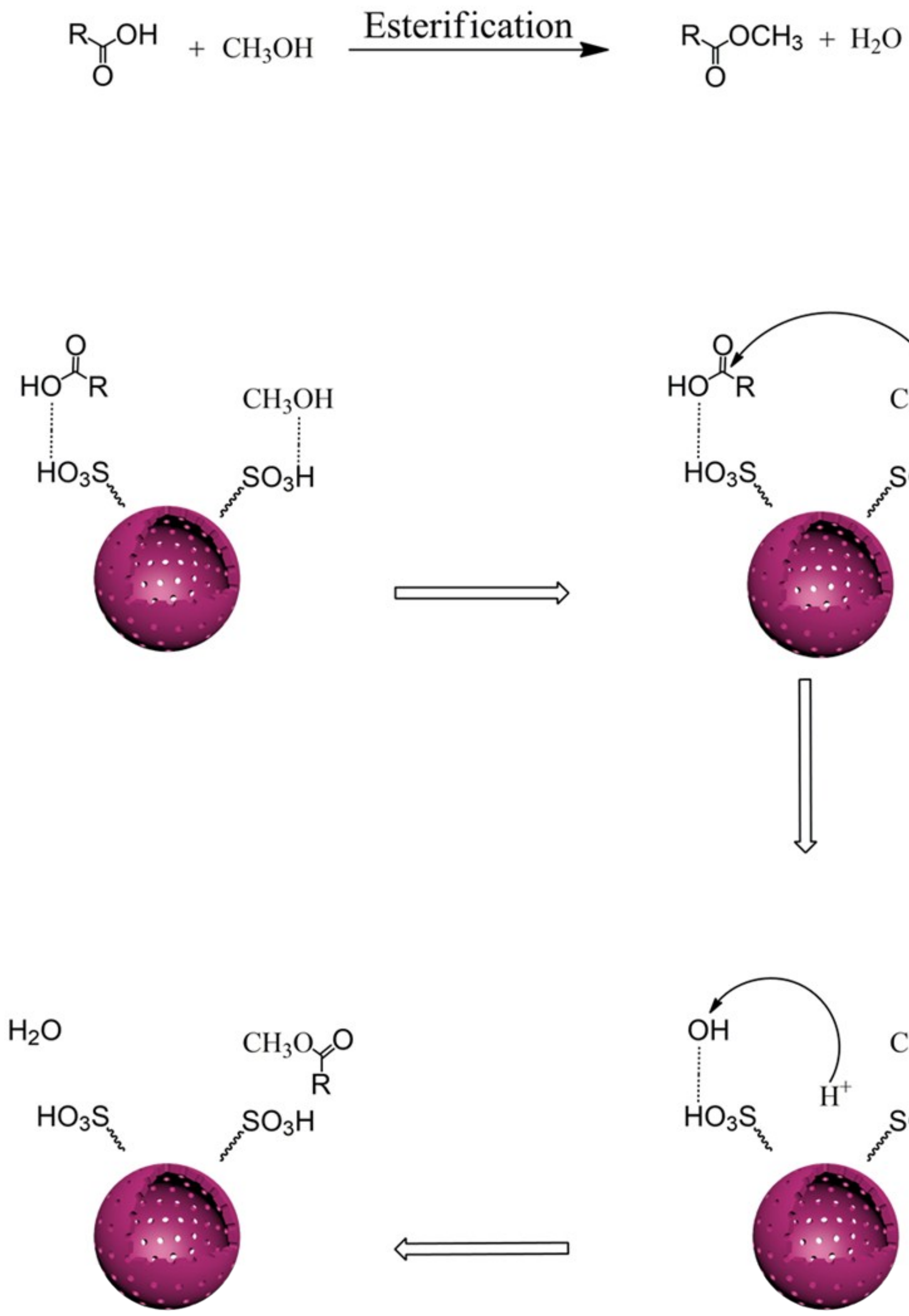

Fig. S9. SHPB-SA catalyzed reaction mechanism of esterification reaction.

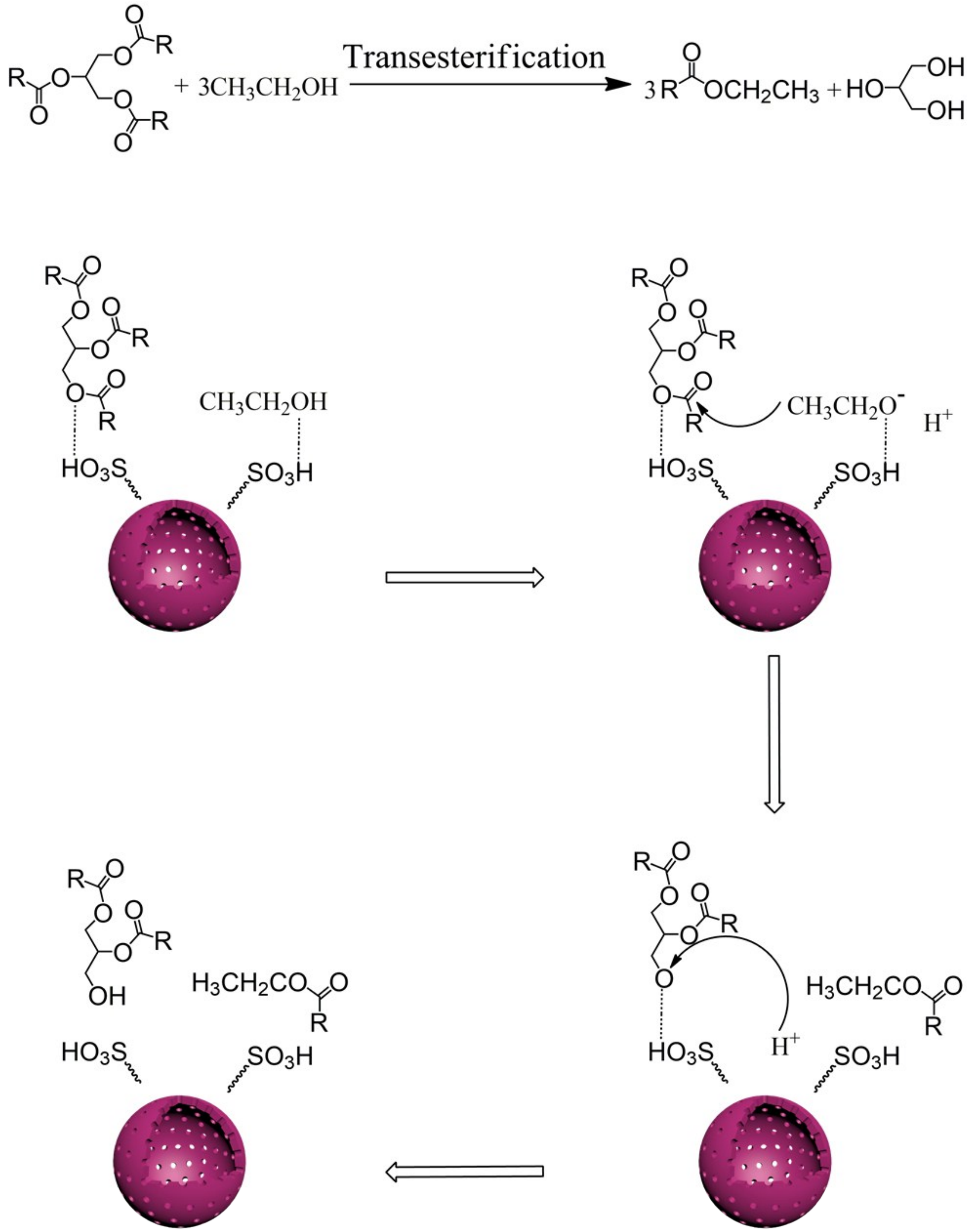

Fig. S10. SHPB-SA catalyzed reaction mechanism of transesterification reaction.

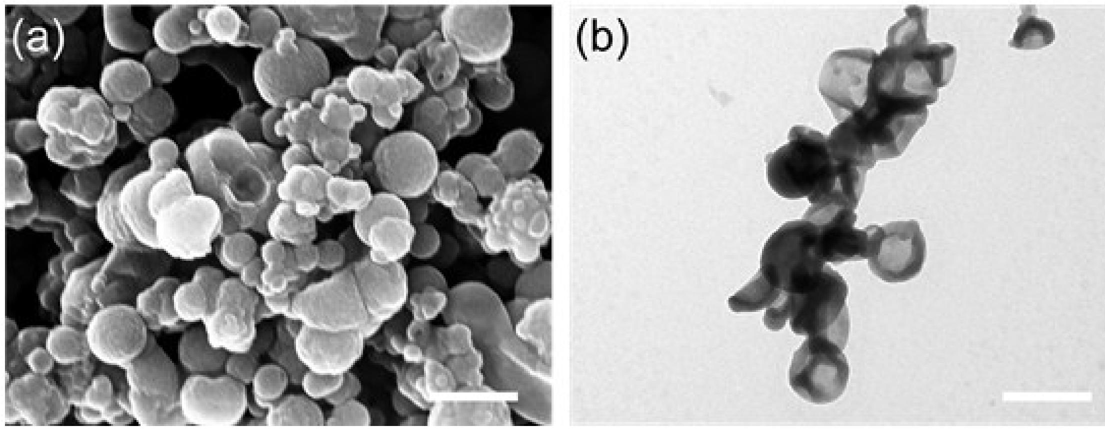

Fig. S11. The SEM and TEM images of the recycled SHPB-SA. The hollow morphology still could be observed. Scale bar, 500 nm.

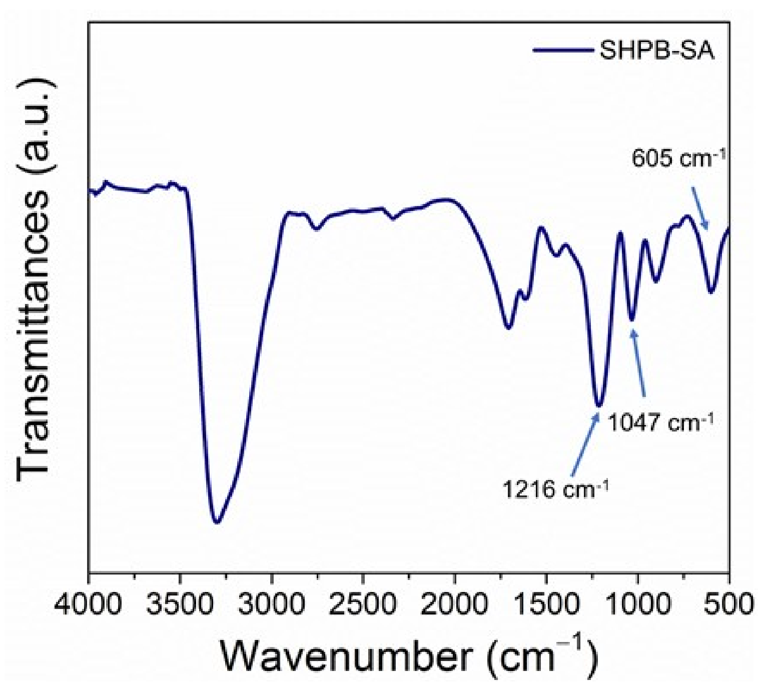

Fig. S12. The FT-IR spectrum of the recycled SHPB-SA.

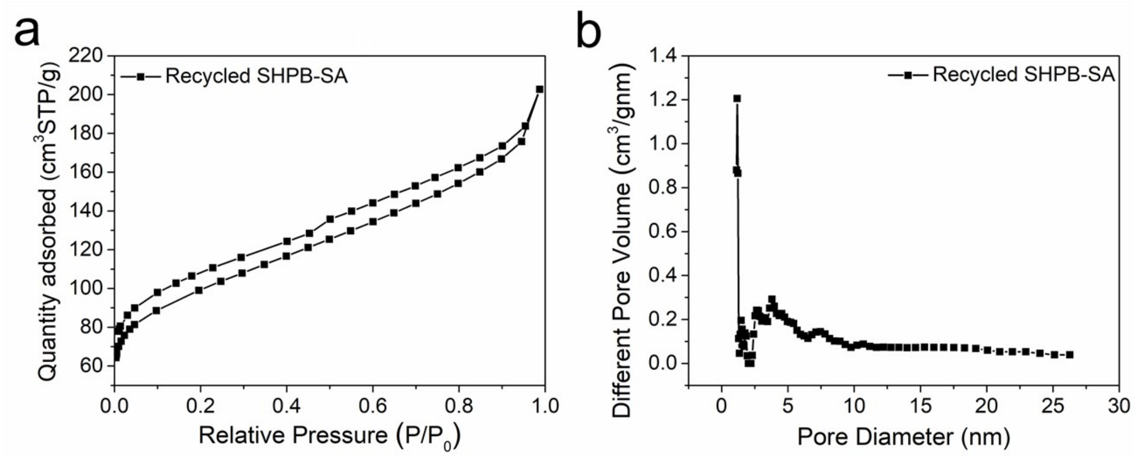

Fig. S13. The BET surface area measurement of the recycled SHPB-SA. The N_2 adsorption–desorption isotherms (a) and pore size distributions calculated using nonlocal density functional theory (NL-DFT) method spectrum (b) of the SHNP-SA after 5 cycles of the transesterification reaction.

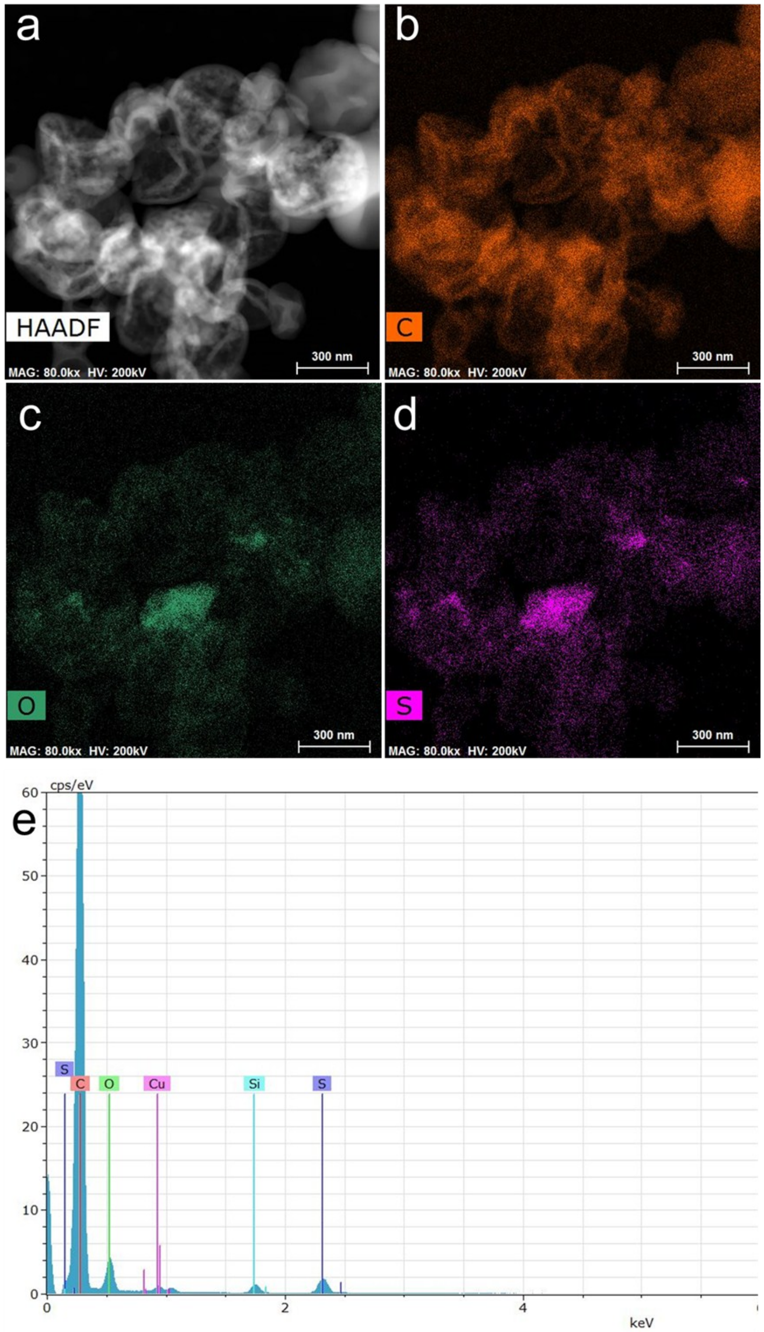

Fig. S14. The EDX mapping results of the recycled SHPB-SA. It could be observed the sulfur could be well maintained after the reactions.

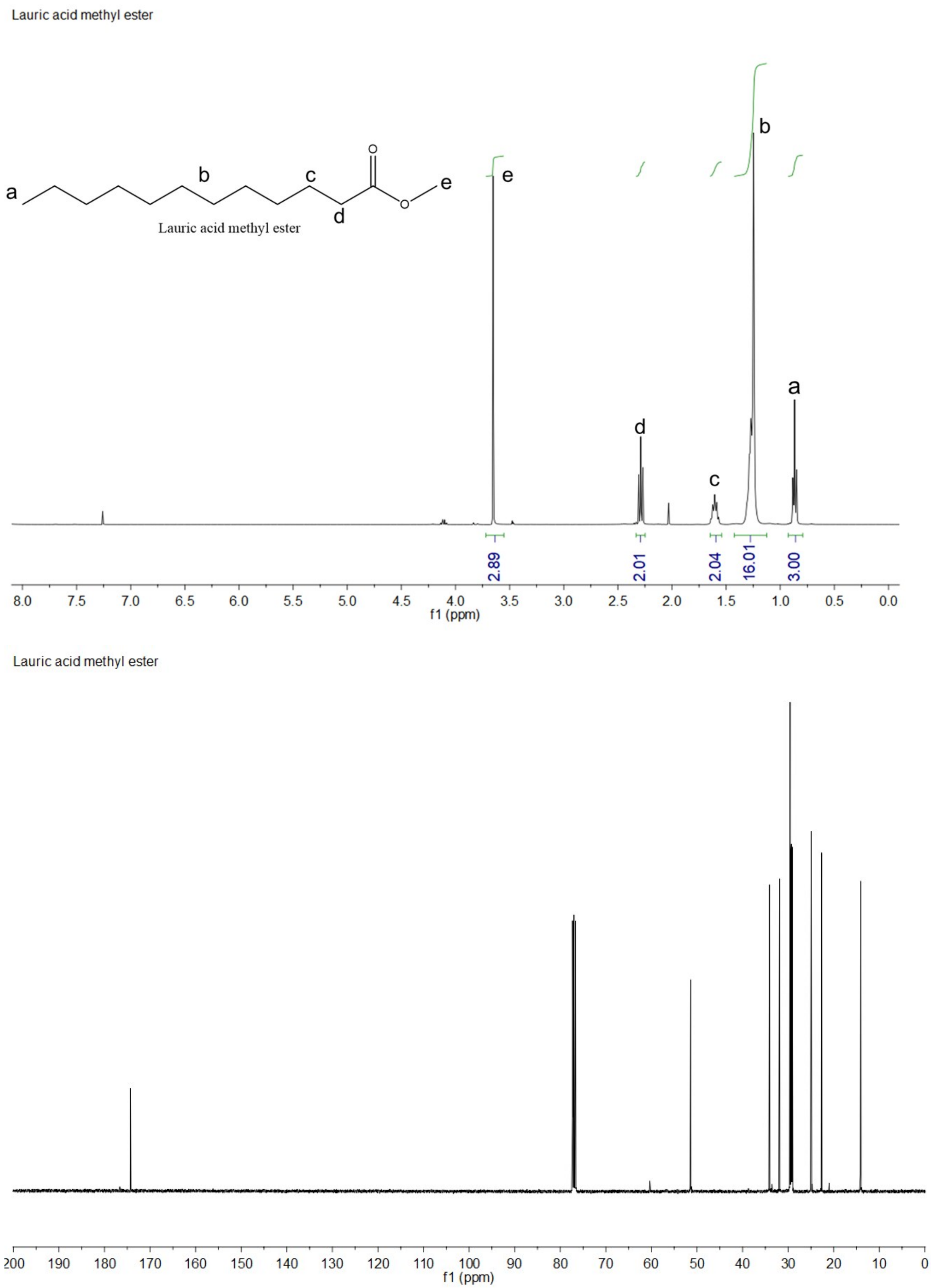

Fig. S15. The [1]H NMR and [13]C NMR spectra of the lauric acid methyl ester.

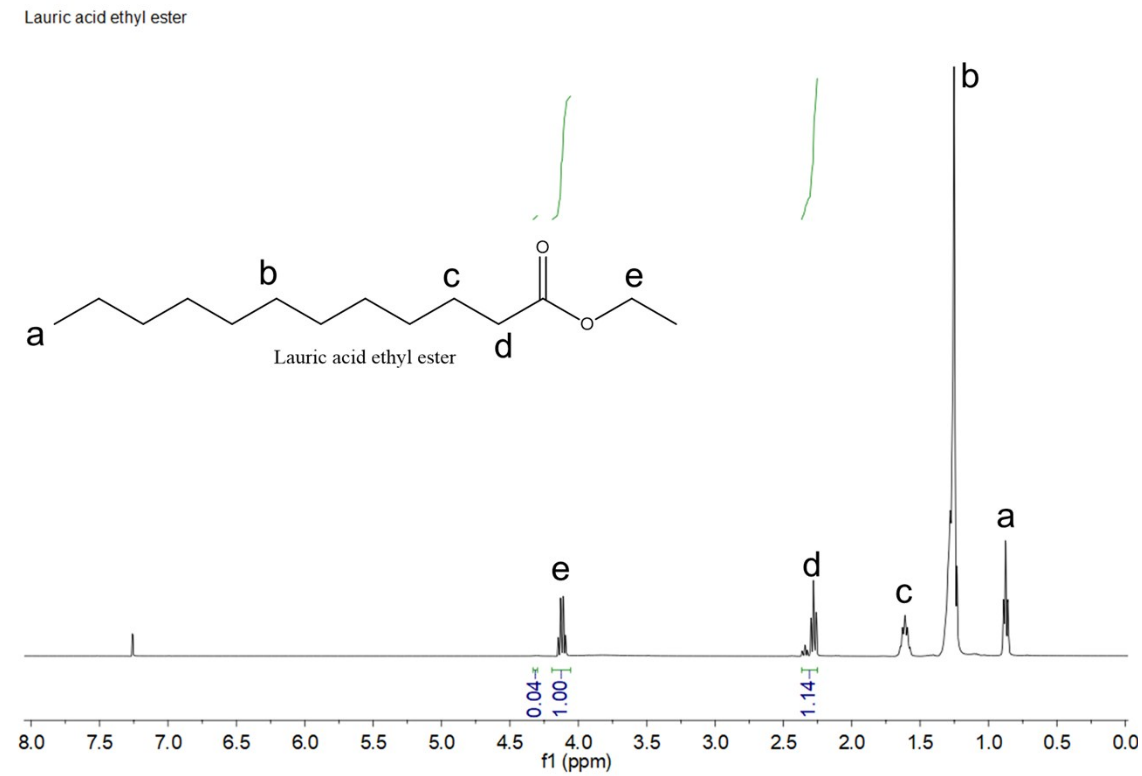

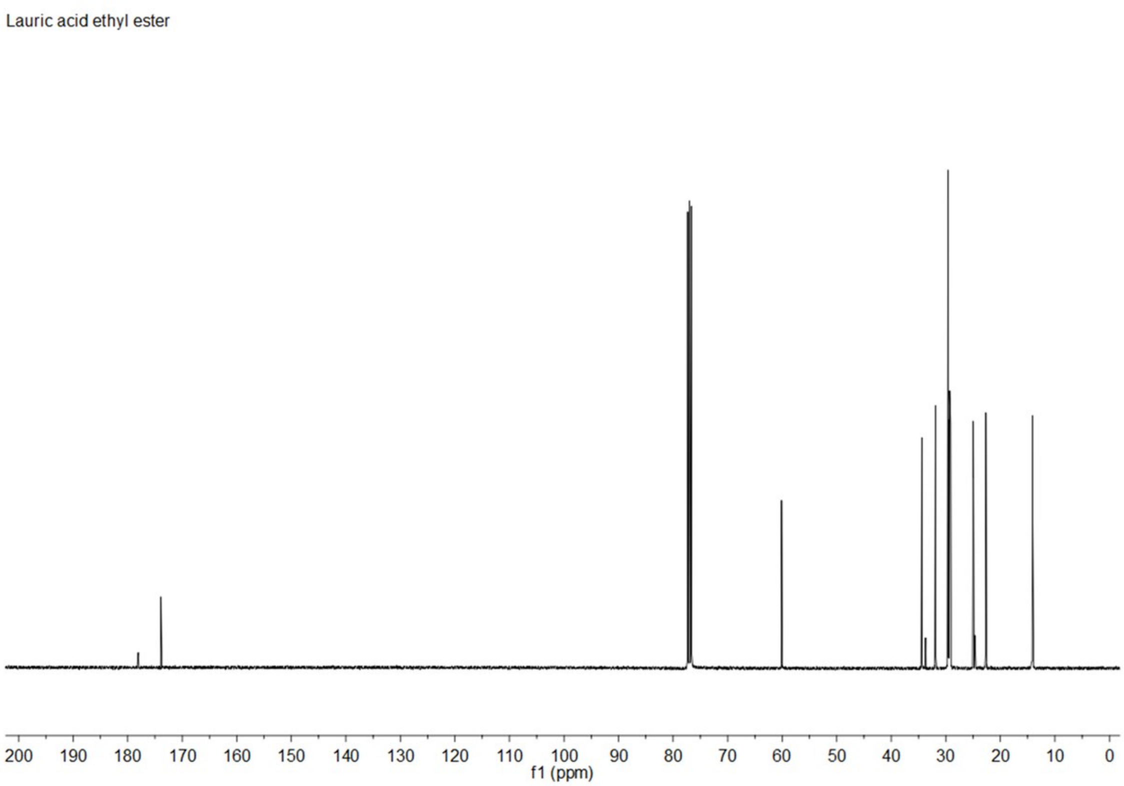

Fig. S16. The ^{1}H NMR and ^{13}C NMR spectra of the lauric acid ethyl ester.

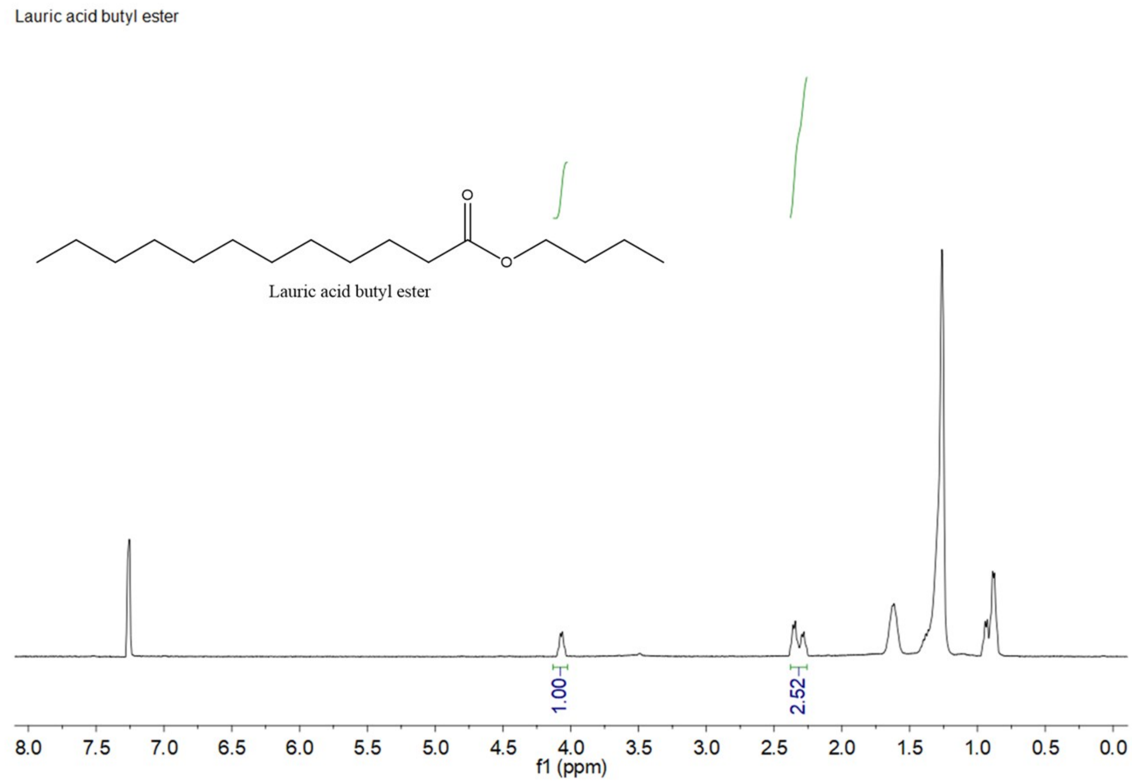

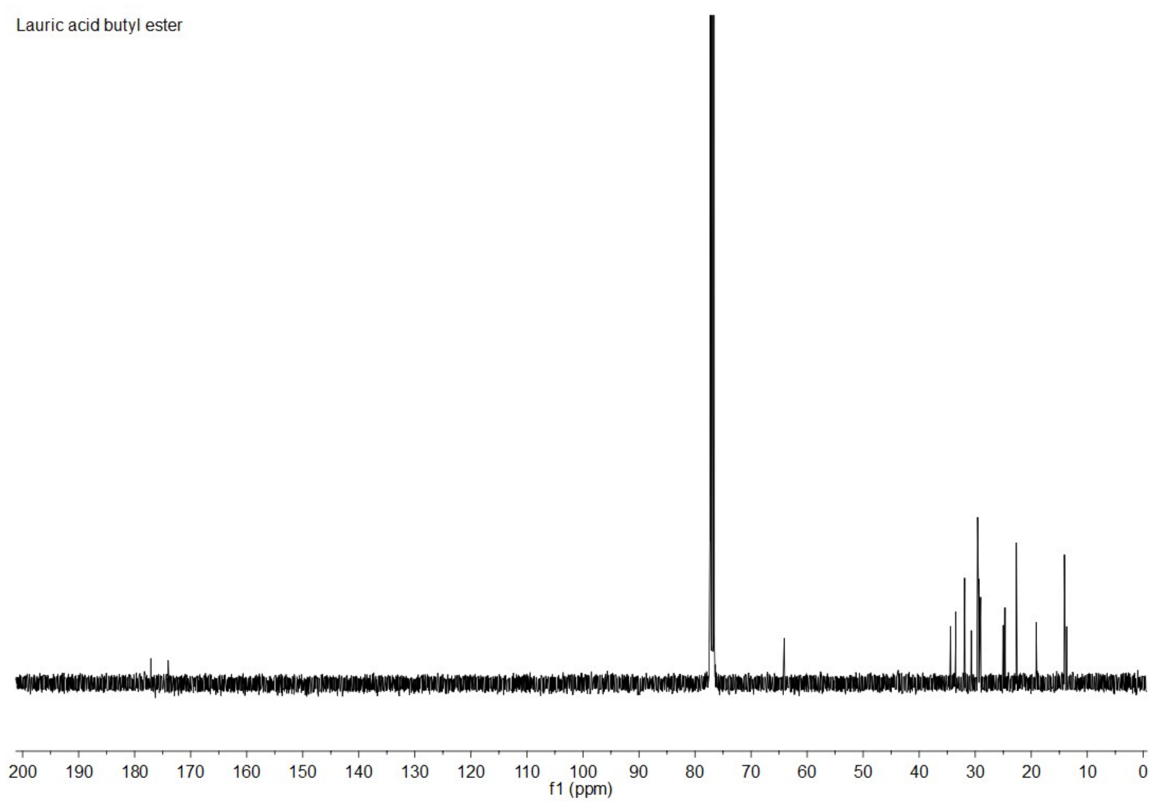

Fig. S17. The ^{1}H NMR and ^{13}C NMR spectra of the lauric acid butyl ester.

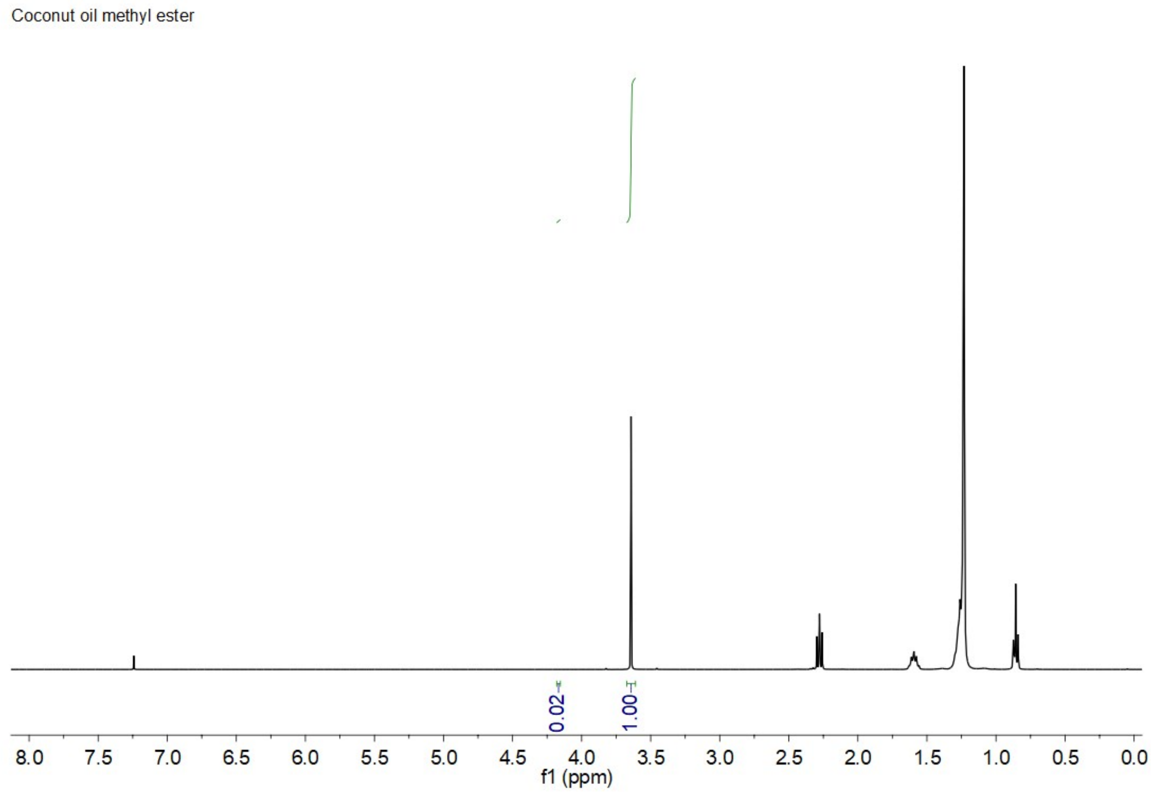

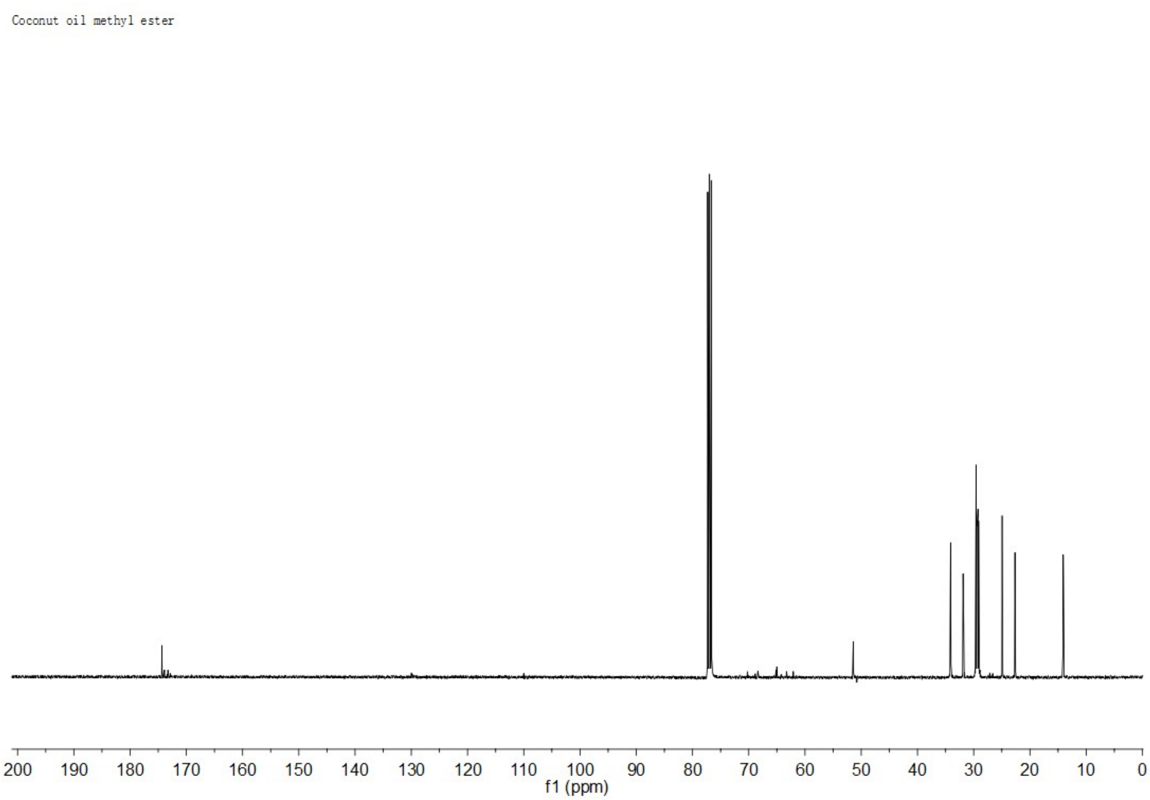

Fig. S18. The ^{1}H NMR and ^{13}C NMR spectra of the coconut oil methyl ester.

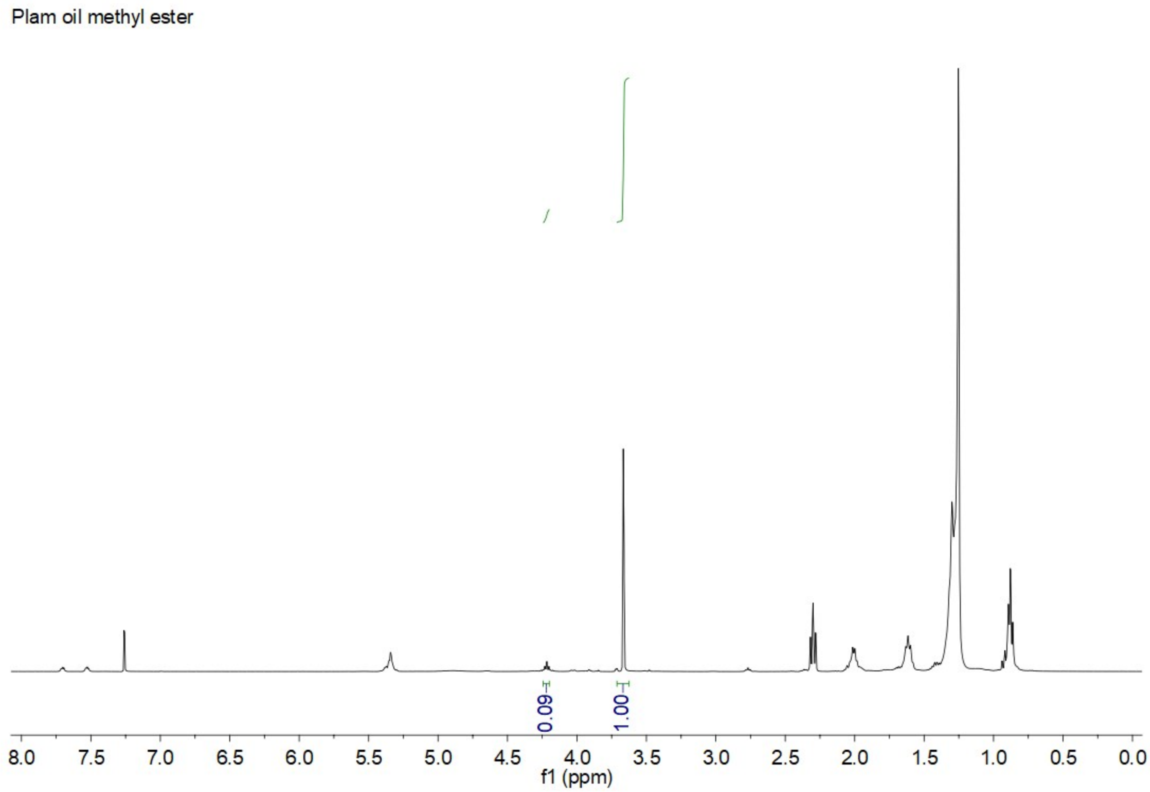

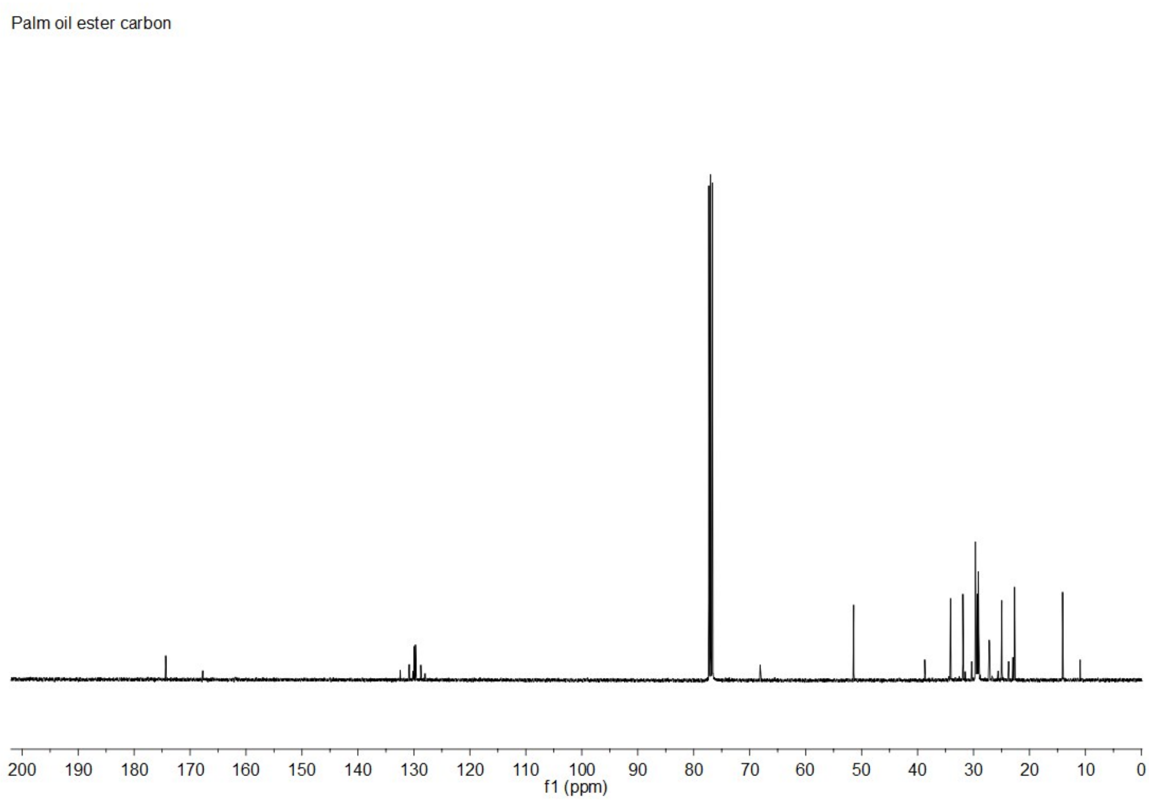

Fig. S19. The ^{1}H NMR and ^{13}C NMR spectra of the palm oil methyl ester.

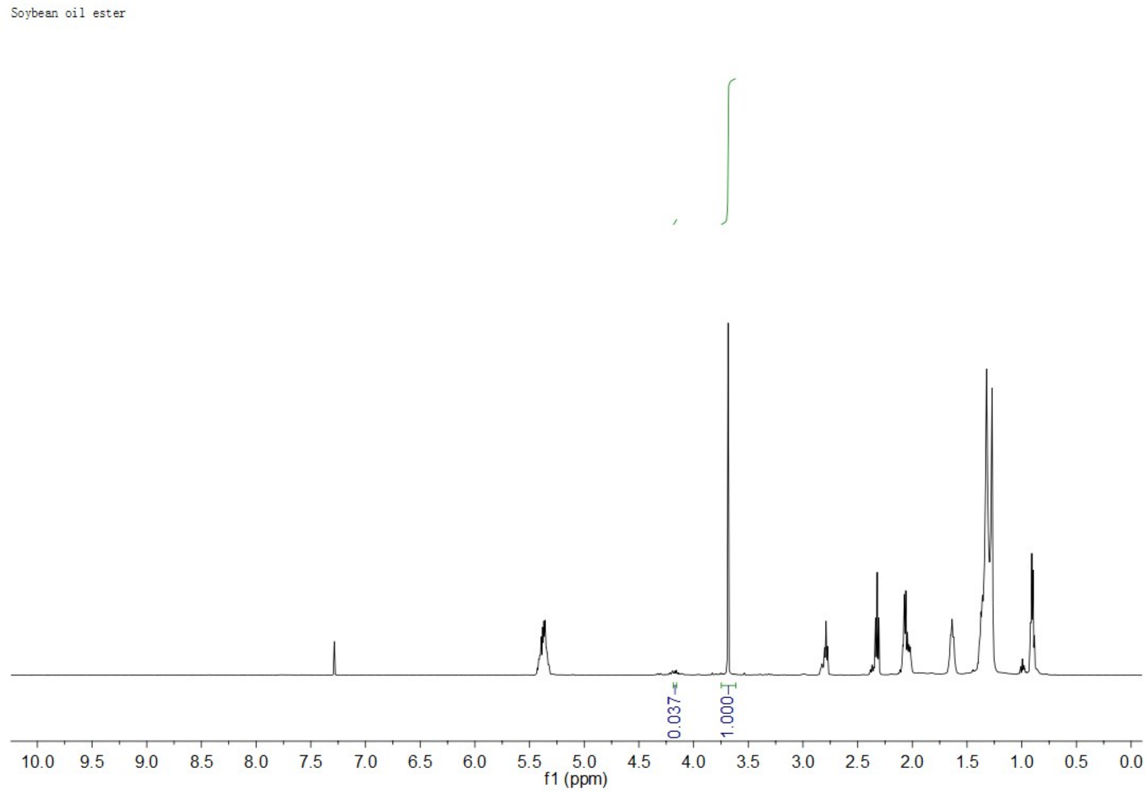

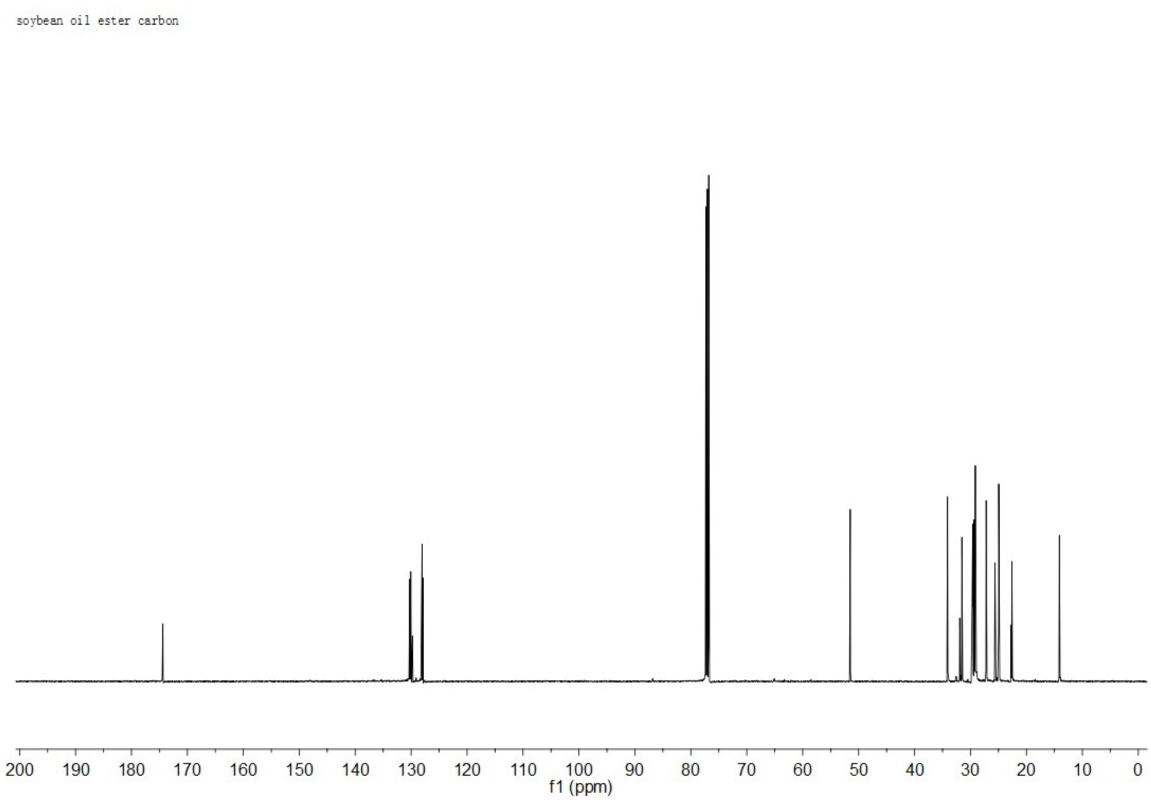

Fig. S20. The ^{1}H NMR and ^{13}C NMR spectra of the soybean oil methyl ester.

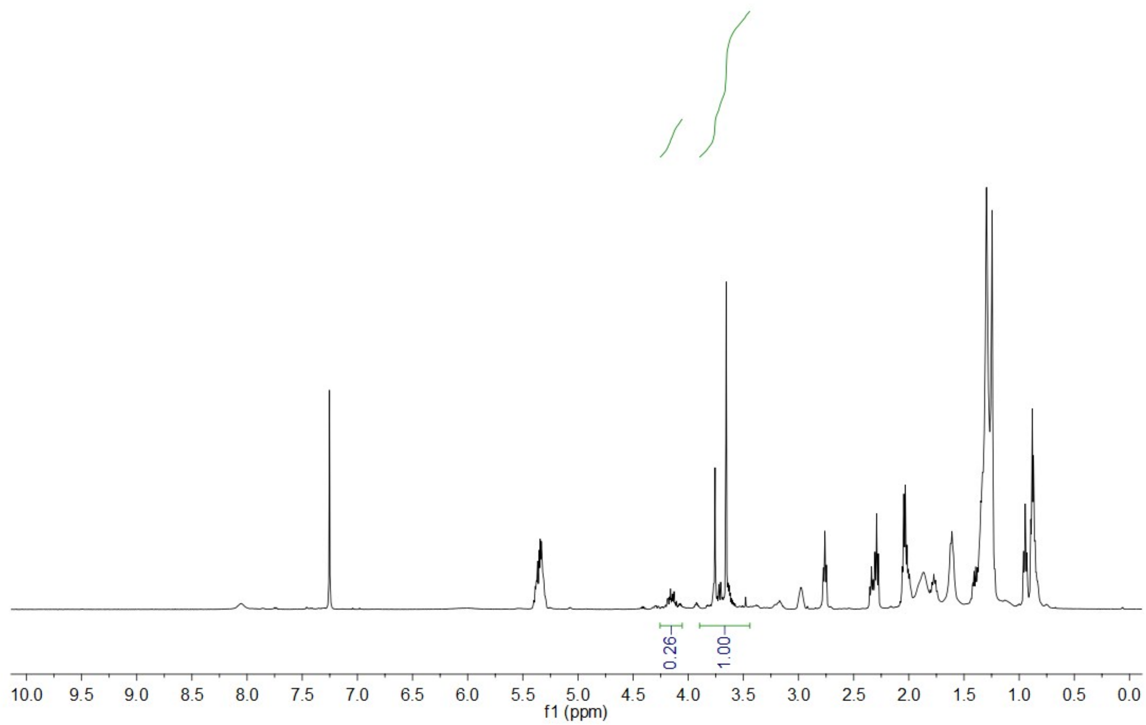

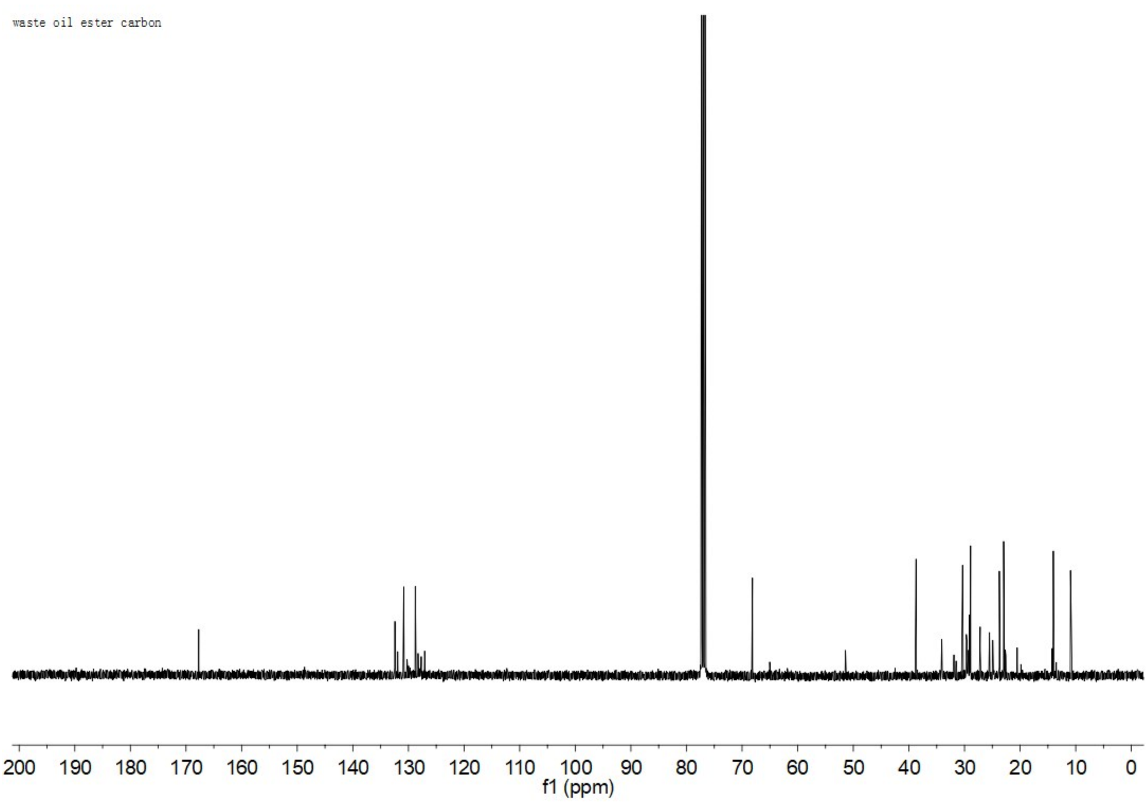

Fig. S21. The ^{1}H NMR and ^{13}C NMR spectra of the waste oil methyl ester.

Table S1. Conventional method for synthesis the hollow polymer spheres with tunable wall-thickness

Raw materials	Template	Wall-thickness control	Morphology	Preparation time (h)*	BET surfaces area[a] (m^2/g)	Ref.[b]
BHB and BHN	No template	Possible	Hollow nanospheres with tunable shell thickness	~36	989	This work
Styrene and divinylbenzene	Hard template SiO_2	Impossible	Hollow nanospheres	~133	626	S1
Terephthalaldehyde and terephthalamidine dihydrochloride	Hard template SiO_2	Impossible	Hollow microspheres/ Bowl	~182	298	S2
Poly(ethylene oxide)-*b*-polystyrene	Soft template	Impossible	Hollow nanospheres	~133	1123	S3
Dopamine	Hard template PS	Impossible	Flower like hollow sphere	~88	27.42	S4
M-phenylenediamine, formaldehyde and ammonium hydroxide	Hard template TEOS	Possible	Hollow nanospheres	~53	484/ 520/ 664 m^2g^{-1}	S5
2,5-dihydroxyterephthalaldehyde and 1,3,5-tris(4-aminophenyl) benzene	No template	Impossible	Hollow microspheres	~144	456	S6
PEO–PPO–PEO, sodium oleate and glucose	Soft template	Possible	Hollow microspheres/ Bowl	~37	871	S7
Polylactide-b-polystyrene	Soft template	Impossible	Hollow nanospheres	~197	806	S8

[a] The highest BET surface area reported in the article. [b] Reference.

[*] The minimum time required for generate the hollow polymeric spheres.

Table S2. The EDX results of the SHSPs before and after the transesterification reactions.

Element	Before *Wt%*	After *Wt%*
C	77.74	85.00
O	14.32	8.33
S	7.94	6.66

References

S1 Z. Jia, K. Wang, B. Tan and Y. Gu, *ACS Catal.*, 2017, **7**, 3693–3702.

S2 N. Wang, G. Cheng, L. Guo, B. Tan and S. Jin, *Adv. Funct. Mater.*, 2019, **29**, 1904781.

S3 T. N. Gao, T. Wang, W. Wu, Y. Liu, Q. Huo, Z. A. Qiao and S. Dai, *Adv. Mater.*, 2019, **31**, 1806254.

S4 H. Wang, Q. Lin, L. Yin, Y. Yang, Y. Qiu, C. Lu and H. Yang, *Small*, 2019, **15**, 1900011.

S5 J. Cheng, X. Zhang, X. Miao, C. Chen, Y. Liu, Y. Chen, J. Lin, S. Chen, W. Wang and Y. Zhang, *Electrochim. Acta*, 2019, **312**, 358–368.

S6 S. Kandambeth, V. Venkatesh, D. B. Shinde, S. Kumari, A. Halder, S. Verma and R. Banerjee, *Nat. Commun.*, 2015, **6**, 6786.

S7 X. Liu, P. Song, J. Hou, B. Wang, F. Xu and X. Zhang, *ACS Sustain. Chem. Eng.* 2018, **6**, 2797–2805.

S8 Z. He, M. Zhou, T. Wang, Y. Xu, W. Yu, B. Shi and K. Huang, *ACS Appl. Mater. Interfaces*, 2017, **9**, 35209–35217.